JACS
JOURNAL OF THE AMERICAN CHEMICAL SOCIETY

Article

Modeling Tryptophan/Indoleamine 2,3-Dioxygenase with Heme Superoxide Mimics: Is Ferryl the Key Intermediate?

Pritam Mondal, and Gayan B. Wijeratne

J. Am. Chem. Soc., **Just Accepted Manuscript** • DOI: 10.1021/jacs.9b10498 • Publication Date (Web): 23 Dec 2019

Modeling Tryptophan/Indoleamine 2,3-Dioxygenase with Heme Superoxide Mimics: Is Ferryl the Key Intermediate?

Pritam Mondal† and Gayan B. Wijeratne*,†

†Department of Chemistry, University of Alabama at Birmingham, Birmingham, AL 35205, United States.

ABSTRACT: Tryptophan oxidation in biology has been recently implicated in a vast array of paramount pathogenic conditions in humans, including multiple sclerosis, rheumatoid arthritis, type-I diabetes, and cancer. This 2,3-dioxygenative cleavage of the indole ring of tryptophan with dioxygen is mediated by two heme enzymes, tryptophan 2,3-dioxygenase (TDO) and indoleamine 2,3-dioxygenase (IDO), during its conversion to *N*-formylkynurenine in the first and rate-limiting step of kynurenine pathway. Despite the pivotal significance of this enzymatic transformation, a vivid viewpoint of the precise mechanistic events is far from complete. A heme superoxide adduct is thought to be the active oxidant in both TDO and IDO, which, following O–O bond cleavage, presumably generates a key ferryl (Fe^{IV}=O) reaction intermediate. This study, for the first time in model chemistry, demonstrates the potential of synthetic heme superoxide adducts to mimic the bioinorganic chemistry of indole dioxygenation by TDO and IDO, challenging the widely accepted categorization of these metal adducts as weak oxidants. Herein, an electronically divergent series of ferric heme superoxo oxidants mediates the facile conversion of an array of indole substrates into their corresponding 2,3-dioxygenated products, while shedding light on an unequivocally occurring, putative ferryl intermediate. The oxygenated indole products have been isolated in ~31% yield, and characterized by LC-MS, ^{1}H and ^{13}C NMR, and FT-IR methodologies, as well as by $^{18}O_{2(g)}$ labeling experiments. Distinctly, the most electron-deficient superoxo adduct is observed to react the fastest, specifically with the most electron-rich indole substrate, underscoring the cruciality of electrophilicity of the heme superoxide moiety in facilitating the initial indole activation step. Comprehensive understanding of such mechanistic subtleties will benefit future attempts in the rational design of salient therapeutic agents, including next generation anticancer drug targets with amplified effectivity.

INTRODUCTION

Tryptophan 2,3-dioxygenase (TDO) and indoleamine 2,3-dioxygenase (IDO) catalyze the rate-limiting first step of kynurenine pathway, in which the indole ring of tryptophan (Trp) is oxidatively cleaved at the 2,3-position to produce *N*-formylkynurenine (NFK) using dioxygen (Chart 1).[1-6] TDO and IDO are two evolutionarily related heme enzymes (TDO is tryptophan-specific, while IDO can dioxygenate a broader scope of substrates with indole moieties, such as melatonin, serotonin, and tryptamine),[7-9] however, unlike a majority of such enzymes,[10-12] their active oxidant is thought to be a heme superoxo adduct (Figure 1), and uniquely require only a single reduction event during complete turnover.[4, 13-14] These heme dioxygenases have been the focal point of multiple human health related recent studies since; (1) accumulated intermediates of kynurenine pathway are known to lead to various disease conditions including multiple sclerosis,[15] AIDS-related dementia,[16] ischemic brain injury,[17] cataract formation,[18] depression,[19-20] Huntington's disease,[21-22] rheumatoid arthritis,[23] and type-I diabetes;[24] (2) IDO serves in a critical immunoregulation role by exerting antimicrobial/antiviral[25] activity via Trp degradation; (3) these enzymes have been recently implicated in cell aging.[26] Most importantly, TDO/IDO have been found to engage in Trp catabolism in human T-cells, aiding tumors to evade anticancer immunosurveillance of the host.[27-30] Thus, TDO/IDO inhibitors are rapidly emerging anti-cancer and/or anti-aging therapeutic agents.[31-37]

Chart 1. Tryptophan 2,3-Dioxygenation to *N*-formylkynurenine Mediated by TDO and IDO Enzymes Using Dioxygen.

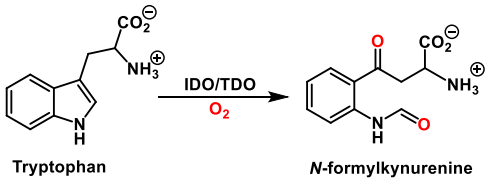

The mechanism through which these enzymes operate has been actively pursued for over half a century, however, the key events/steps still remain elusive. The lack of such mechanistic understanding can significantly impede the ability to develop novel therapeutic agents with enhanced activity. A base-catalyzed mechanistic proposal had been widely accepted and reproduced in the literature,[3, 38] however, recent studies including the structural characterization of human IDO have led to its fall, since (1) the active site of IDO lacked a distal histidine that was proposed to abstract the indole ring proton of Trp (Figure 1B),[1, 39] and (2) *N*-methyltryptophan was found to be a slow, but active substrate, whereas in a base-catalyzed scenario it would be inactive.[40] Accordingly, the mechanistic viewpoint has rapidly

evolved, leading to proposals that differentiate the initial heme superoxide attack on Trp between (1) an electrophilic-, or (2) a radical-addition (Figure 1C).[4, 41-44] Intriguingly, both of these proposed mechanisms converge at a common intermediate step: the formation of a ferryl intermediate and the indole epoxide (Figure 1C). Lending credence, a ferryl intermediate has been spectroscopically observed during human IDO turnover, where the formation and decay of a ferryl-based Fe=O resonance Raman feature has been evidenced at 799 cm^{-1}.[45-47] A handful of synthetic TDO/IDO models exist,[48-53] out of which, only a few has utilized synthetic heme mimics.[54-56] Nevertheless, insights into the identity and properties of the active metal oxidant, key reaction intermediates, and/or pivotal mechanistic events are severely lacking.[57-61]

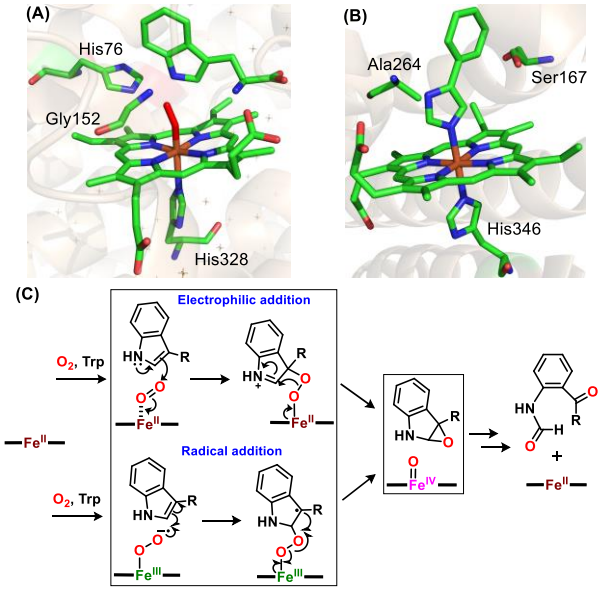

Figure 1. Crystallographically characterized (A) ternary complex of human TDO that includes the Trp substrate and the heme-bound dioxygen moiety (PDB: 5TI9),[2] and (B) active site of human IDO (inhibitor bound; PDB: 2DOT) exhibiting the absence of a distal histidine residue.[1] (C) Current mechanistic proposals for the dioxygenation of tryptophan by IDO and TDO, where the initial indole activation step is either an electrophilic or a radical addition.

In sharp contrast to their biological,[11, 62] and non-heme[63-64] counterparts, synthetic heme superoxo adducts have long known to be weak oxidants.[65-66] Accordingly, their organic substrate oxidation reactivity is gravely understudied,[67] and models of enzymes with a heme superoxide active species are virtually non-existent. To this end, we herein describe the first series of synthetic heme superoxide models that closely mimic the tryptophan oxidation (bio)chemistry of TDO/IDO enzymes, cleaving the 2,3-double bond of an array of indole substrates using dioxygen (Scheme 1). This work, also for the first time in model chemistry, sheds light on the ferryl species involved in this mechanism, and presents multiple spectroscopic and reactivity evidences that support its occurrence as a reaction intermediate. Further, the fastest dioxygenation reaction rate is observed between the most electron-deficient superoxide adduct, and the most electron-rich substrate, corroborating an addition of the indole to the electrophilic heme superoxide in a rate-limiting initial substrate activation step. Isotopic labeling experiments involving $^{18}O_{2(g)}$ reveal intriguing insights into key mechanistic details of this reaction, suggesting the possibility of substrate dissociation upon the completion of the initial monooxygenation step. The dioxygenated final organic products have also been isolated and unambiguously identified. In addition to the significant advancement in TDO/IDO modeling presented in this work, to the best of our knowledge, this marks the first instance where unprecedented substrate oxidation capabilities of heme superoxide adducts are revealed, warranting reevaluation of their conventional classification as sluggish oxidants.

Scheme 1. Generalized Reaction Scheme Depicting Structural Variations of Heme Systems and Indole Substrates Involved in this Study.

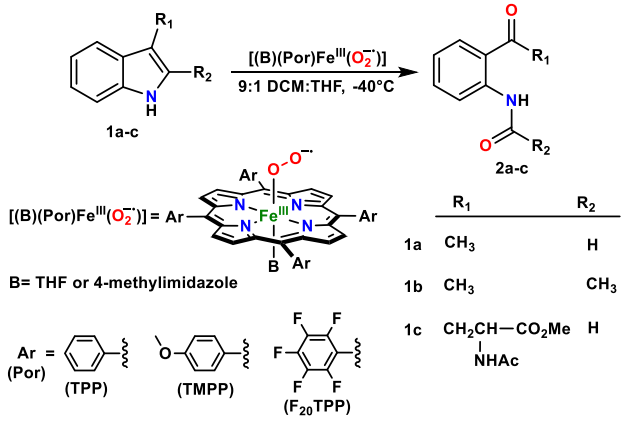

RESULTS AND DISCUSSION

Formation and Dioxygenation Reactivity of Heme Superoxide Adducts. We have thoughtfully selected three porphyrinate systems for this study, which offer significantly disparate electronic atmospheres for the heme iron center: $F_{20}TPP$ ($F_{20}TPP$ = 5,10,15,20-tetrakis(pentafluorophenyl)-porphyrin), TPP (TPP = 5,10,15,20-tetraphenylporphyrin), and TMPP (TMPP = 5,10,15,20-tetrakis(4-methoxyphenyl)-porphyrin). The ferrous heme complex, **[(THF)$_2$(TPP)Fe^{II}]**, exhibited significant electronic absorption perturbations from 426 (Soret; ε = 16 × 10^5 $M^{-1}cm^{-1}$), 536 (ε = 6.2 × 10^4 $M^{-1}cm^{-1}$) and 558 (ε = 6.5 × 10^4 $M^{-1}cm^{-1}$) nm to 416 (Soret; ε = 10 × 10^5 $M^{-1}cm^{-1}$) and 540 (ε = 9.0 × 10^4 $M^{-1}cm^{-1}$) nm in 9:1 DCM:THF solvent mixture at –80 °C upon the bubbling of dry $O_{2(g)}$, indicating the formation of the EPR-silent, end-on ferric superoxo species, **[(THF)(TPP)Fe^{III}($O_2^{\bullet-}$)]** (Figure 2).[12, 68] Isotope-sensitive ν(Fe–O) and ν(O–O) resonance Raman frequencies for this species were centered at 579 ($\Delta^{18}O_2$ = –26) and 1170 ($\Delta^{18}O_2$ = –60) cm^{-1}, respectively (Figure 2). Subsequent addition of 2 equiv of 4 methylimidazole (Im) led to the formation of the Im-coordinated superoxo adduct, **[(Im)(TPP)Fe^{III}($O_2^{\bullet-}$)]** (418 (Soret; ε = 7.5 × 10^5 $M^{-1}cm^{-1}$) and 543 (ε = 6.5 × 10^4 $M^{-1}cm^{-1}$) nm);[69-72] ν(Fe–O): 577 ($\Delta^{18}O_2$ = –23) and ν(O–O): 1170 ($\Delta^{18}O_2$ = –56) cm^{-1} (Figure 2).[72-74] Similarly, the rest of the ferric superoxo compound series was prepared and

characterized: **[(THF)(F$_{20}$TPP)Fe^{III}(O$_2^{-\bullet}$)]**, **[(Im)(F$_{20}$TPP)Fe^{III}(O$_2^{-\bullet}$)]**, **[(THF)(TMPP)Fe^{III}(O$_2^{-\bullet}$)]** and **[(Im)(TMPP)Fe^{III}(O$_2^{-\bullet}$)]** (Figures S1 and S2).[12]

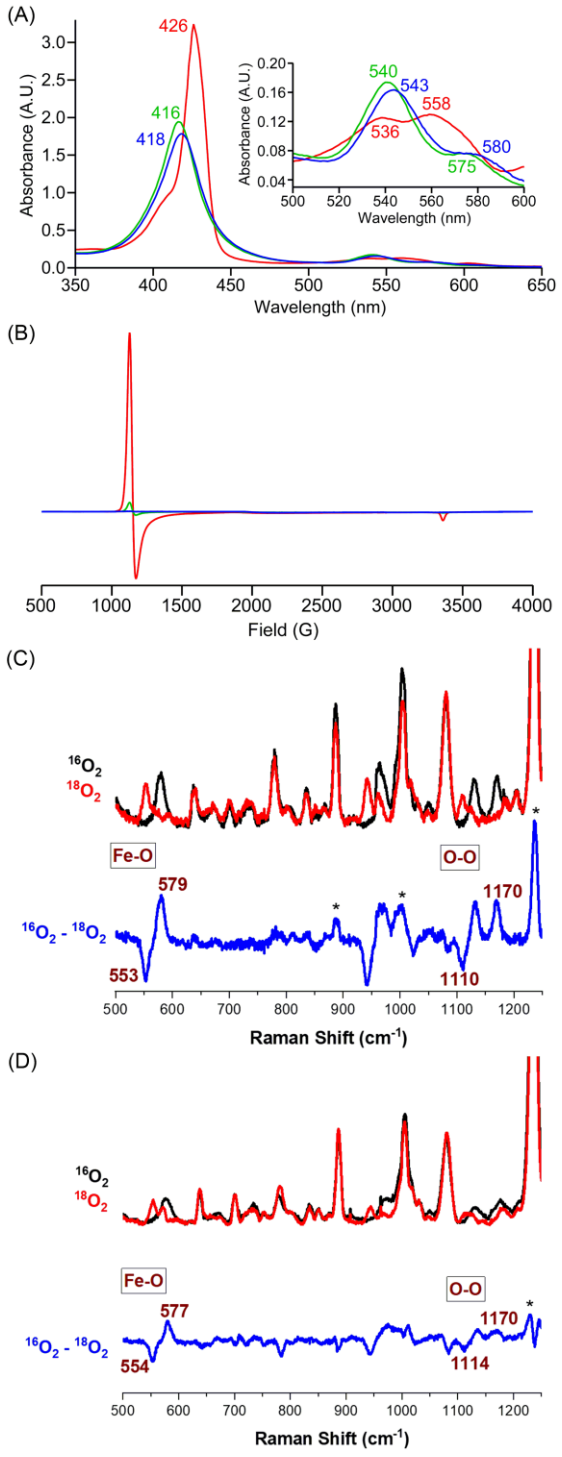

Figure 2. (A) UV-vis spectra for 10 μM solutions of **[(THF)$_2$(TPP)Fe^{II}]** (red), **[(THF)(TPP)Fe^{III}(O$_2^{-\bullet}$)]** (green), and **[(Im)(TPP)Fe^{III}(O$_2^{-\bullet}$)]** (blue) at –80 °C; (B) EPR spectra for frozen 2 mM solutions of **[(THF)(TPP)Fe^{III}(O$_2^{-\bullet}$)]** (green), and **[(Im)(TPP)Fe^{III}(O$_2^{-\bullet}$)]** (blue) compared with that of a **[(TPP)Fe^{III}(Cl)]** (red) at 7 K; resonance Raman spectra (λ_{ex} = 406.7 nm) of 2 mM (C) **[(THF)(TPP)Fe^{III}(O$_2^{-\bullet}$)]** and (D) **[(Im)(TPP)Fe^{III}(O$_2^{-\bullet}$)]** prepared with $^{16}O_{2(g)}$ (black) and $^{18}O_{2(g)}$ (red) (*due to subtraction of intense heme bands). Solvent: 9:1 DCM:THF.[75]

To probe the reactivity of these ferric superoxide adducts, 100 equiv of the indole substrates were added in at –80 °C; however, no spectral changes were evident. Markedly, upon warming this mixture up to –40 °C, the superoxide adducts initiated reactivity with added indole substrates, with the intermediacy of a distinct heme species. For example, for **[(THF)(TPP)Fe^{III}(O$_2^{-\bullet}$)]**, a subtle, but prominent red shift (from 416 to 417 nm) followed by a blue shift (417 to 414 nm) of the Soret band was observed along with overall decrease in the absorption intensity (Figure 3A) in the presence of 3-methylindole (Scheme 1; **1a**). Such sequential biphasic spectral changes were even more prominent for the reaction between **[(Im)(TPP)Fe^{III}(O$_2^{-\bullet}$)]** and **1a** (Figure 3B). Similar changes were also observed for **[(THF)(F$_{20}$TPP)Fe^{III}(O$_2^{-\bullet}$)]** (Figure S4), **[(Im)(F$_{20}$TPP)Fe^{III}(O$_2^{-\bullet}$)]** (Figure S4), **[(THF)(TMPP)Fe^{III}(O$_2^{-\bullet}$)]** (Figure S3) and **[(Im)(TMPP)Fe^{III}(O$_2^{-\bullet}$)]** (Figure S3) at –40 °C (or –55 °C (*vide infra*)). As well, other substituted indoles shown in Scheme 1 (i.e., **1b** and **1c**) displayed similar reactivity (Figures S5 and S6). Noticeably, no reaction was observed with indole, 2-methylindole, or 1,3-dimethylindole. This lack of reactivity is well precedented by previous studies, where a 3-position substituent was found to be essential for dioxygenation, while *N*-substituted indoles exhibited either very slow or no reactivity.[40, 54, 76] In fact, the latter observation was thought to be "evidence" for the previously accepted, now obsolete base-catalyzed mechanism of TDO/IDO.[76] We note here that the decay rates of the heme superoxide complexes in the absence of substrate were at least an order of magnitude slower than the indole oxidation rates, and that self-decay does not possess any distinct reaction intermediates (Figure S8).

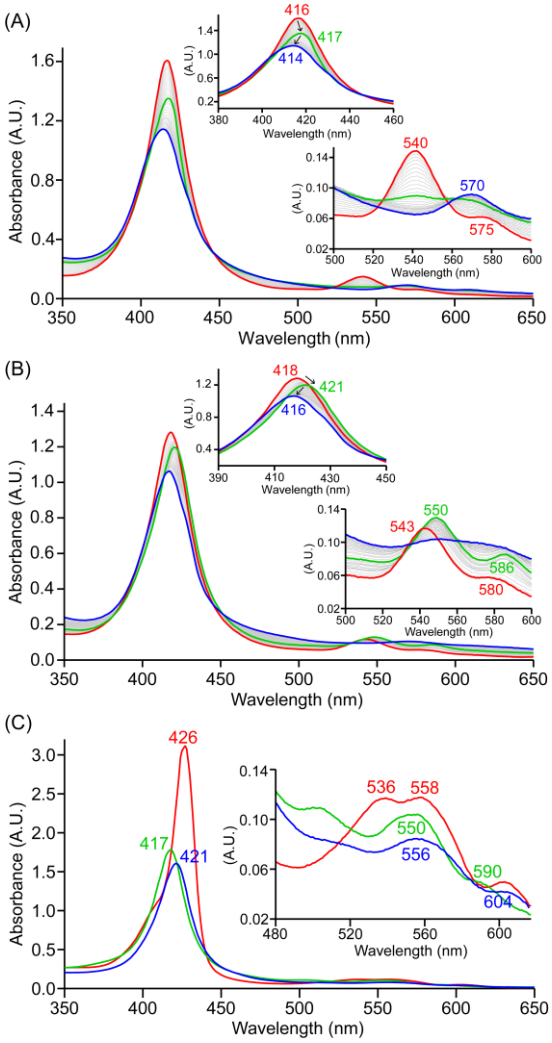

Figure 3. Electronic absorption spectral changes observed during the reaction of a 10 μM 9:1 DCM:THF solution of (A) **[(THF)(TPP)Fe^{III}(O$_2^{-\bullet}$)]** and (B) **[(Im)(TPP)Fe^{III}(O$_2^{-\bullet}$)]** with 100 equiv of 3-methylindole at –40 °C (Red = initial ferric superoxo complex; green = intermediate species; blue = final ferric product). (C) Electronic absorption spectral features of 10 μM **[(THF)$_2$(TPP)Fe^{II}]** (red), independently prepared **[(TPP)Fe^{IV}(O)]** (green) and **[(Im)(TPP)Fe^{IV}(O)]** (blue) in 9:1 DCM:THF at –40 °C. Insets show the expanded Soret and Q-band regions, and arrows indicate the direction of peak transition.

Scheme 2. Schematic Representation of the Independent Generation of Six-coordinate Fe^{IV}=O (ferryl) Complexes.

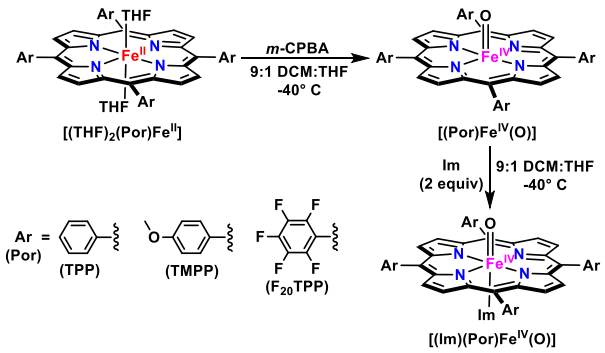

Characterization of the Putative Fe^{IV}=O (Ferryl) Intermediate and Mechanistic Details. Inspired by the unambiguous spectroscopic observation of a heme-based reaction intermediate, and the proposed ferryl intermediate in the TDO/IDO mechanistic proposals (*vide supra*), we set to probe the plausibility of the putative formation of a ferryl intermediate. In this, we have generated authentic ferryl adducts of all three heme systems, **[(Im)(TPP)Fe^{IV}(O)]**, **[(Im)(F$_{20}$TPP)Fe^{IV}(O)]**, and **[(Im)(TMPP)Fe^{IV}(O)]**, by reacting the corresponding Fe^{II} complexes with *m*-CPBA, and the subsequent addition of Im at –40 °C (Scheme 2; Figures 3 and S9).[77-79] Remarkably, the Soret band positions of the independently generated authentic ferryl intermediates were strikingly similar to those of the corresponding reaction intermediates (Figure 3; Figure S9), albeit the Q-band regions exhibited either a mixture of features and/or the peak positions were not clearly distinguishable. This reaction intermediate was also observed to be EPR-silent, as would be expected for a ferryl adduct (Figure S7).[77, 80] To further interrogate this observation in detail, we carried out low-temperature ^{2}H NMR studies utilizing the pyrrole-position deuterated F$_{20}$TPP-*d*$_8$ (see experimental section for details). **[(THF)$_2$(F$_{20}$TPP-*d*$_8$)Fe^{II}]** and **[(THF)(F$_{20}$TPP-*d*$_8$)Fe^{III}(O$_2^{-\bullet}$)]** exhibited a single ^{2}H NMR feature at $\delta_{pyrrole}$ = 89.2 and $\delta_{pyrrole}$ = 8.8 ppm, respectively, as would be expected according to literature precedence (Figure 4).[81] The addition of 3-methylindole into **[(THF)(F$_{20}$TPP-*d*$_8$)Fe^{III}(O$_2^{-\bullet}$)]**, and subsequent increment in temperature from –80 °C to –55 °C led to the immediate formation of a new diamagnetic ^{2}H NMR feature at $\delta_{pyrrole}$ = 3.2 ppm (Figure 4), which is identical to that of the authentic ferryl adduct, while being in close agreement with previous reports.[77, 81] Finally, when the indole oxidation reaction was carried out in the presence of excess triphenylphosphine (PPh$_3$) at –40 °C, triphenylphosphine oxide (O=PPh$_3$) formation was observed in the expense of indole oxidation product formation, as confirmed by ^{31}P NMR (Figure S11).[82] Separate control experiments were carried out in the absence of heme complex, dioxygen, or indole substrate, none of which demonstrated PPh$_3$ oxidation (Figures S12 – S14). Thus, the (1) excellent agreement of Soret, and (2) low-temperature ^{2}H NMR spectroscopic features, while (3) being EPR-silent, and (4) exhibiting triphenylphosphine oxidation impart strong corroboration that the observed reaction intermediate is most likely the anticipated ferryl species, resembling similar observations in the IDO mechanism.[45] To the best of our knowledge, this is the first instance where any evidence in support of the anticipated, biologically-relevant ferryl intermediate has been presented for indole oxidation with any model system. In fact, high-valent heme intermediates have never been observed for any reactivity landscape initiated by synthetic heme superoxides.

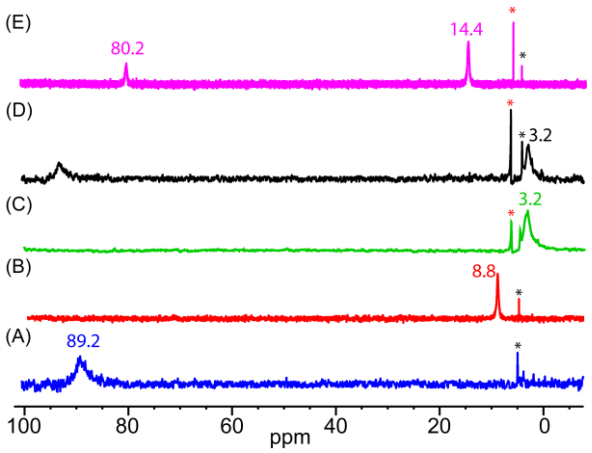

Figure 4. ^{2}H NMR spectral data in 9:1 DCM:THF for (A) **[(THF)$_2$(F$_{20}$TPP-*d$_8$*)Fe^{II}]** at –80° C, (B) **[(THF)(F$_{20}$TPP-*d$_8$*)Fe^{II}(O$_2^{-\bullet}$)]** at –80 °C, (C) authentic ferryl intermediate, **[(THF)(F$_{20}$TPP-*d$_8$*)Fe^{IV}(O)]**, and (D) reaction intermediate between **[(THF)(F$_{20}$TPP-*d$_8$*)Fe^{III}(O$_2^{-\bullet}$)]** and 3-methylindole at –55 °C, and (E) the final heme product at room temperature. (*solvent peaks (black) and an instrumental glitch (red)).

Patent differences in reaction rates among **[(THF)(TPP)Fe^{III}(O$_2^{-\bullet}$)]**, **[(THF)(F$_{20}$TPP)Fe^{III}(O$_2^{-\bullet}$)]**, and **[(THF)(TMPP)Fe^{III}(O$_2^{-\bullet}$)]** were also observed, in that, **[(THF)(F$_{20}$TPP)Fe^{III}(O$_2^{-\bullet}$)]** reacted the fastest, while **[(THF)(TMPP)Fe^{III}(O$_2^{-\bullet}$)]** was the slowest (Figure 5). Indeed, **[(THF)(F$_{20}$TPP)Fe^{III}(O$_2^{-\bullet}$)]** initiated reactivity with indole substrates even at –55 °C, while others required the increment in reaction temperature up to –40 °C. As seen in Figure 5, the kinetic traces collected at Soret wavelengths are clearly biphasic, indicating the fomation and decay of a perceptible intermediate. Intruigingly, for **[(THF)(F$_{20}$TPP)Fe^{III}(O$_2^{-\bullet}$)]** both of these phases are much more rapid compared to **[(THF)(TPP)Fe^{III}(O$_2^{-\bullet}$)]** or **[(THF)(TMPP)Fe^{III}(O$_2^{-\bullet}$)]**, revealing superior reactivity of both the superoxo adduct, and the (ferryl) intermediate. Moreover, the most electron-rich indole substrate, 2,3-dimethyl indole reacts the fastest with all three superoxides. These findings in concert suggest that an attack from the indole substrate on the electrophilic iron superoxo adduct is most likely the initial step of the mechanism. The feasibility of such an attack is in line with the significant "ferrous-oxy" character possessed by these synthetic superoxide adducts.[83] Similar trends have also been observed for heme-modified TDO enzyme models, where electron-withdrawing heme substituents increased the rate of tryptophan oxidation.[84]

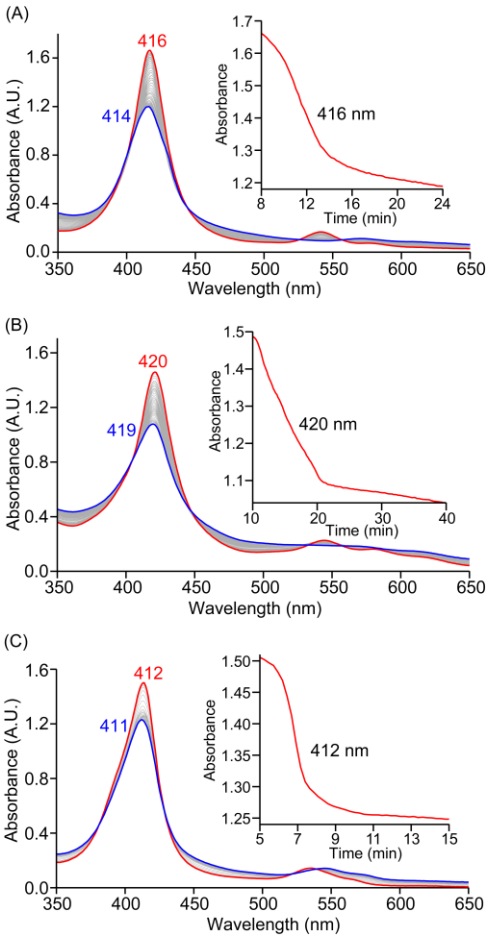

Figure 5. UV-vis spectral changes in 9:1 DCM:THF at –40 °C for the reaction of 10 μM (A) **[(THF)(TPP)Fe^{III}(O$_2^{-\bullet}$)]** (B) **[(THF)(TMPP)Fe^{III}(O$_2^{-\bullet}$)]** and (C) **[(THF)(F$_{20}$TPP)Fe^{III}(O$_2^{-\bullet}$)]** with 100 equiv of 3-methylindole (Red = initial ferric superoxo complex; blue = final ferric product; insets show kinetic time traces for Soret regions).

The rate-limiting regions for TDO/IDO have been discussed in detail,[44] and are both proposed to be pre-ferryl. For TDO, the initial attack on the heme superoxide is the slow-most step, making the ferryl intermediate virtually unobservable. In contrast, IDO encompasses the ferryl species in its slowest step, allowing its detailed characterization.[44-46] With this background, the rate-limiting events for these synthetic heme superoxide adducts presumably incorporate both the initial superoxide attack and ferryl formation, permitting the determination of a clear interdependency between the reaction rates and the heme electronic structure, while allowing the characterization of the (ferryl) intermediate. Accordingly, under pseudo-first-order reaction conditions (50 – 300 equiv of 3-methylindole), the rate of indole dioxygenation by **[(THF)(TPP)Fe^{III}(O$_2^{-\bullet}$)]** displayed linear dependence on the indole substrate concentration, leading to a second order rate constant of 0.47 M^{-1} s^{-1} (Figure 6). Noteworthily, no reactivity was observed if the superoxide adducts were warmed up to –40 °C prior to the addition of substrates, reasonings for which, are currently unclear.

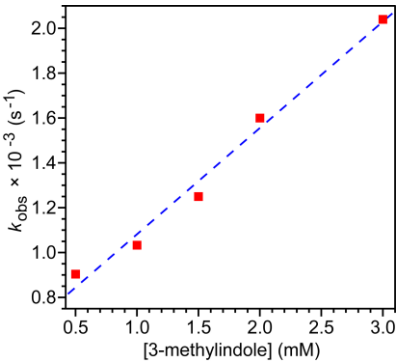

Figure 6. The dependence of pseudo-first-order dioxygenation rate constants (initial rate fits) on the 3-methylindole substrate concentration for 10 μM **[(THF)(TPP)Fe^{III}(O$_2^{-\bullet}$)]** in 9:1 DCM:THF at –40 °C.

Bulk-scale Indole Oxygenation Reactions and Overall Reaction Landscape. To further rationalize the hypothesized indole 2,3-dioxygenation chemistry, we designed scaled-up reactions using **[(THF)(TPP)Fe^{III}(O$_2^{-\bullet}$)]**, permitting rigorous characterization of the desired organic products by ^{1}H and ^{13}C NMR, FT-IR, and LC-MS methods (Figures S15 – S20). For example, when 3-methylindole (**1a**) was subjected to heme superoxide mediated oxidation, *ortho*-formamidoacetophenone (**2a**) was found to be the major product. Likewise, the predominant organic product following the oxidation of **1b** and **1c** (Scheme 1) were revealed to be **2b** and **2c**, respectively.[85] However, the maximum yield of product isolated capped at ~31%; the balance of the added substrate was leftover, i.e., unreacted. For imidazole-coordinated superoxide adducts, as also previously reported,[54] both the reaction rates and the yield of the final dioxygenated product were diminished (yield = ~20%), presumably due to competitive interactions exerted by imidazole (Figure S21). We note that the present study, therefore, offers the first fully characterized series of organic products for a heme dioxygenase enzyme mimic. Interestingly, when isotopically-labeled $^{18}O_{2(g)}$ was utilized, the mass of (major) product **2c** shifted from 293.11 to 297.12 *m/z*, indicating the incorporation of two ^{18}O atoms (Figure S18). When a 1:1 $^{16}O_{2(g)}$:$^{18}O_{2(g)}$ mixture was used to oxidize the indole substrate **1c**, a 1:1:1 ratio among the 2 x ^{16}O:^{16}O^{18}O:2 x ^{18}O incorporated **2c** products was observed (Figure S19), shedding light on the stepwise oxygen insertion mechanism at play (similar to TDO/IDO; see Figure 1C). This crucial, unprecedented result also indicates the likelihood of indole epoxide dissociation following the initial oxygenation step (Figure 1C), which presumably dictates the modest reaction yields. This observation underscores the importance of the extended protein structure that likely restricts a similar substrate dissociation in TDO/IDO, allowing the generation of stoichiometric dioxygenated products. In line with the UV-vis experiments (*vide supra*), none of the substrates that lacked 3-position indole ring substituents or the proton on the indole *N*-atom produced the desired product in bulk reactions. The final heme product in these dioxygenation reactions was characterized to be either the oxo-bridged (*μ*-oxo) diferric compound, **[{(TPP)Fe^{III}}$_2$(*μ*-O)]**, or the bis-Im ferric complex, **[(Im)$_2$(TPP)Fe^{III}]$^+$**, in the absence and presence of Im, respectively (Scheme 3; Figures S23 and S24).

Scheme 3. Plausible Pathways for the Overall Dioxygenation Reaction.

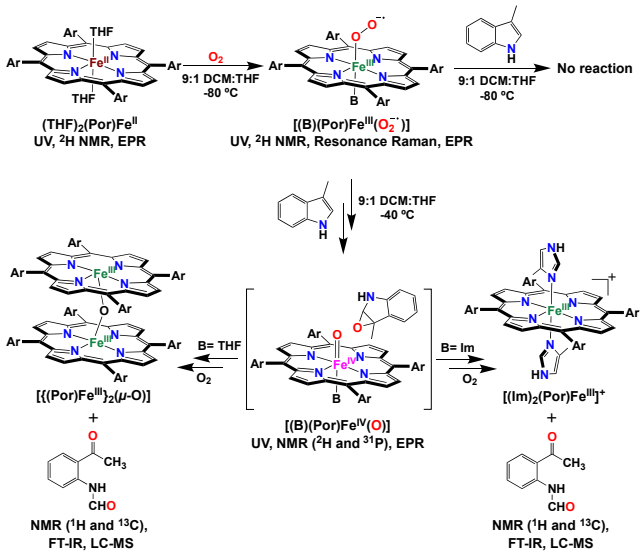

CONCLUSIONS

TDO/IDO-dependent tryptophan 2,3-dioxygenation in biology is fundamental for a battery of human health related concerns, including some of the most supreme challenges in human pathogenesis.[15-24, 31-37] Both TDO and IDO are heme enzymes, and their active oxidant is thought to be a heme superoxide adduct.[4, 10-13] However, the current literature on heme superoxide intermediates, irrespective of protein or synthetic model-based, acutely lack a direct linkage to indole dioxygenation. To this end, this study communicates the first report where a medley of synthetic heme superoxide and indole substrate models have been utilized to mimic the aforementioned tryptophan oxidation chemistry of TDO and IDO heme enzymes. The thermal instability of such dioxygen-derived synthetic heme superoxide models has warranted the use of cryogenic conditions, and upon warming up the superoxide/indole mixtures from –80 to –40 °C (or –55 °C), the indole substrates were observed to undergo 2,3-bond cleaving dioxygenation, yielding ~31% product. Interestingly, we report the detection of a low-temperature reaction intermediate (UV-vis, ^{2}H NMR, EPR, and PPh$_3$ oxidation), which we propose to be the biologically-relevant ferryl species (Figure 1C).

The electronic properties of both the heme oxidants and the indole substrates employed in this interrogation offer clear trends in rates of indole oxidation, strongly suggesting that an indole addition to an electrophilic heme superoxide moiety is the initial step of the reaction. Our findings here are therefore in favor of one of the proposed mechanisms for TDO/IDO (Figure 1C), paralleling previous studies on heme-modified TDOs.[84] This initial indole addition step is also rate-limiting, and in support, the rate of indole oxidation is linearly dependent on the indole concentration. Our scaled-up approach has allowed the detailed

characterization of oxidized organic products by ^{1}H NMR, ^{13}C NMR, FT-IR, and LC-MS analyses, as well as $^{18}O_{2(g)}$ labeled studies that uncover strong evidence supporting a stepwise/sequential dioxygen insertion mechanism, as would be expected for TDO/IDO. In contrast to TDO/IDO, however, the indole epoxide intermediate in these model systems presumably escape following the first oxygen insertion step, likely due to the absence of sterically encumbering protein mass that limit/prevent substrate dissociation in nature. The final heme product is Fe(III) rather than the mechanistically expected Fe(II) species. This anomaly is possibly due to the rapid oxidation of the resultant Fe(II) (from indole oxidation) by dissolved dioxygen in solution; indeed the oxo-bridged (μ-oxo) diferric compound, **[{(TPP)Fe^{III}}$_2$(μ-O)]**, is known to be the main product of the reaction between Fe(II) and dioxygen at non-cryogenic temperatures.[86-87] In conclusion, we have succeeded in the efficient modeling of biological tryptophan 2,3-dioxygenation using synthetic heme-based superoxo models, however, further interrogations are warranted for definitive mechanistic conclusions, and/or for fully comprehending the identity of key intermediates, and unique substrate specificities observed in this study that draw close resemblance to TDO/IDO enzymes.

EXPERIMENTAL SECTION

Materials and Methods. All commercially available chemicals were purchased at the highest available purity, and used as received unless otherwise stated. Air-sensitive compounds were handled either under an argon atmosphere using standard Schlenk techniques, or in an Mbraun Unilab Pro SP (<1 ppm O_2, <1 ppm H_2O) nitrogen-filled glovebox. All organic solvents were purchased at HPLC-grade or better. DCM and THF were degassed (by bubbling argon gas for 30 min at room temperature) and dried (by passing through a 60 cm alumina column) using an Inert Pure Solv MD 5 (2018) solvent purification system. These solvents were then stored in amber glass bottles inside the glovebox over 4 Å molecular sieves at least for 72 hrs prior to use. The purity of O_2 gas used was >99%, and was further dried by passage through a 12" column containing drierite and 5 Å molecular sieves. Benchtop UV-vis experiments were carried out using an Agilent Cary 60 spectrophotometer equipped with a liquid nitrogen chilled Unisoku Cool-Spek UV USP-203-B cryostat. A 2 mm path length quartz cell cuvette modified with an extended glass neck with a female 14/19 joint and stopcock was used to perform all UV-vis experiments. Resonance Raman samples were excited at 406.7 nm, using a Coherent I90C-K Kr+ ion laser, while the sample was immersed in a liquid nitrogen cooled (77 K) EPR finger dewar (Wilmad). Power was ~4 mW at the sample. Data were recorded while rotating the sample manually to minimize photodecomposition. The spectra were recorded using a Spex 1877 CP triple monochromator with a 600 groves/mm holographic spectrograph grating, and detected by an Andor Newton CCD cooled to -80 °C. Spectra were calibrated on the energy axis to citric acid. The resonance Raman data was processed using the spectroscopy software SpectraGryph version 1.2 (Dr. Friedrich Menges Software-Entwicklung, Oberstdorf, Germany) and Origin 2019b software. ^{1}H NMR and ^{13}C NMR spectra at room temperature were recorded on a Bruker Avance III-HD 500 MHz NMR Spectrometer. ^{31}P NMR and low-temperature ^{2}H NMR spectroscopic studies were carried out on a Bruker DRX 400 MHz NMR Spectrometer. All NMR spectra were recorded in 5-mm (outer diameter) tubes. The chemical shifts were reported as δ (ppm) values calibrated to natural abundance deuterium or proton solvent peaks. Infrared (IR) vibrational spectra were collected on a Bruker FT-IR spectrometer (Vertex 70) at room temperature. A SCIEX 5600 Triple-Tof mass spectrometer (SCIEX, Toronto, Canada) was used to analyze the mass profiles of the organic products. The IonSpray voltages for positive modes were +/- 5000 V, and the declustering potential was 80 V. Ionspray GS1/GS2 and curtain gases were set at 40 psi and 25 psi, respectively. The interface heater temperature was maintained at 400 °C. Electron paramagnetic resonance (EPR) spectra were collected in 4 mm (outer diameter) quartz tubes using an X-band Bruker EMX-plus spectrometer coupled to a Bruker ER 041 XG microwave bridge, and a continuous-flow liquid helium cryostat (ESR900) controlled by an Oxford Instruments TC503 temperature controller (experimental conditions: microwave frequency = 9.41 GHz; microwave power = 0.2 mW; modulation frequency = 100 kHz; modulation amplitude = 10 G; temperature = 7 K). 5,10,15,20-tetraphenylporphyrin iron(III) chloride, **[(TPP)Fe^{III}Cl]**, and 5,10,15,20-tetrakis(4-methoxyphenyl)-porphyrin, **H$_2$(TMPP)** were purchased from commercial sources. The syntheses of **H$_2$(F$_{20}$TPP)**,[88] **H$_2$(F$_{20}$TPP)-*d$_8$***,[89] and 1,3-dimethylindole[90] were carried out according to previously published methods. Metalation of the porphyrinates to generate **[(TMPP)Fe^{III}Cl]**, **[(F$_{20}$TPP)Fe^{III}Cl]**, and **[(F$_{20}$TPP-*d$_8$*)Fe^{III}Cl]**, and the subsequent reduction to **[(THF)$_2$(Por)Fe^{II}]** complexes were carried out by following previously reported procedures.[81] **[{(TPP)Fe^{III}}$_2$(μ-O)]** and 'naked' **[(THF)$_2$(TPP)Fe^{III}]SbF$_6$** compounds were synthesized as previously reported.[91-93]

Formation of the Heme Superoxo Complexes, [(B)(Por)Fe^{III}($O_2^{-\bullet}$)], where B = THF or Im; Por = the porphyrinate supporting ligand. Generation of the superoxo complexes, **[(B)(Por)Fe^{III}($O_2^{-\bullet}$)]**, was carried out following a literature-adapted procedure.[70-71, 73, 81] In a typical experiment, a 10 μM 9:1 DCM:THF solution (1 mL) of **[(THF)$_2$(Por)Fe^{II}]** was added into a 2 mm pathlength Schlenk cuvette inside the glovebox, and was sealed using a rubber septum. Upon cooling down inside the UV-vis cryostat stabilized at –80 °C, this solution was bubbled with dry dioxygen gas using a needle, and the complete formation of the superoxide complexes, **[(THF)(Por)Fe^{III}($O_2^{-\bullet}$)]**, was monitored by UV-vis spectroscopy. Excess $O_{2(g)}$ was removed by three vacuum/Ar purge cycles, and the subsequent addition of 2 equiv of 4-methylimidazole (Im; in 50 μL of 9:1 DCM:THF) resulted in the 6-coordinate superoxide complexes, **[(Im)(Por)Fe^{III}($O_2^{-\bullet}$)]** (Figures 2A and S1).

Resonance Raman Sample Preparation. In a typical experiment, 300 μL of the ferrous heme complex, **[(THF)$_2$(Por)Fe^{II}]** (2 mM in 9:1 DCM:THF), was placed in a 9 mm NMR tube, and was sealed with a rubber septum. Following cooling down to –80 °C, dry $O_{2(g)}$ (or $^{18}O_{2(g)}$) was bubbled through the solution mixture using a three-way gas-tight syringe in order to generate the corresponding superoxide complex, **[(B)(Por)Fe^{III}($O_2^{-\bullet}$)]**. Immediately

following the heme superoxide formation, the solutions were frozen in liquid N_2, and the tubes were flame-sealed.

Spectroscopic Reactivity Studies of [(B)(Por)Fe^{III}($O_2^{-\bullet}$)] with Indole Substrates. The indole substrates (1 mM, 50 μL) were added into the 2 mm pathlength cuvette containing **[(B)(Por)Fe^{III}($O_2^{-\bullet}$)]** (10 μM, 1 mL) in 9:1 DCM:THF using a Hamilton gas-tight syringe at –80 °C, and the cuvette contents were quickly mixed with Ar bubbling. No spectral changes were observed at –80 °C. Then, the temperature of the cryostat was raised up to –40 °C (Figures 3, S3, S5 and S6) or –55 °C (Figure S4), upon which, the reactions with the indole substrates were initiated, and the corresponding spectral changes were recorded. The self-decay of the superoxide complexes was also monitored at –40 °C without the addition of any indole substrates (Figure S8).

Kinetic Analysis of Indole Dioxygenation. For variable substrate concentration kinetic analyses, different indole concentrations were utilized, and the aforementioned methodology followed to initiate the reaction. The kinetic data was analyzed utilizing the initial rate method, where the first 20% of the data was fit to obtain the reaction rates (Figure 6).

Generation of the Authentic [(Im)(Por)Fe^{IV}(O)] Intermediates. [(Im)(Por)Fe^{IV}(O)] (ferryl) intermediates were prepared following a previously published method by Karlin and co-workers.[77] In a typical procedure, 1 equiv of *m*-CPBA was added into a 10 μM solution of **[(THF)$_2$(Por)Fe^{II}]** in 9:1 DCM:THF (1mL) at –40 °C to yield **[(Por)Fe^{IV}(O)]** adducts; successive addition of 2 equiv of Im resulted in the formation of Im ligated ferryl derivatives, **[(Im)(Por)Fe^{IV}(O)]** (Scheme 2). These complexes were characterized by UV-vis spectroscopy (Figures 3C and S9) and NMR spectroscopy, and are in excellent agreement with the literature reports.[78, 81, 94-96] Figures 3C and S9 presents a comparison between the UV-vis features of authentic **[(Im)(Por)Fe^{IV}(O)]** complexes and those of the corresponding indole oxidation reaction intermediates.

Synthesis and Characterization of [(F_{20}TPP-*d*$_8$)Fe^{III}Cl] and [(THF)$_2$(F_{20}TPP-*d*$_8$)Fe^{II}]. The synthesis of **H_2(F_{20}TPP)-*d*$_8$** ligand was carried out according to literature procedures.[89] Generation of **[(F_{20}TPP-*d*$_8$)Fe^{III}Cl]** and the subsequent reduction to **[(THF)$_2$(F_{20}TPP-*d*$_8$)Fe^{II}]** were carried out by following previously reported methods.[81]

[(F_{20}TPP-*d*$_8$)Fe^{III}Cl]: UV-vis (0.1 mM in CH_2Cl_2): 410 (Soret; ε = 1.2×10^5 M^{-1}cm^{-1}), 503 (ε = 1.5 × 10^4 M^{-1}cm^{-1}) and 629 (ε = 7.7 × 10^3 M^{-1}cm^{-1}) nm; ^{2}H NMR ($CHCl_3$, 298 K): $\delta_{pyrrole}$ = 82.5 ppm; ESI-MS: {[(M-Cl)+CH_3CN]$^+$} *m/z* = 1077.55 (calc. 1077.05).

[(THF)$_2$(F_{20}TPP-*d*$_8$)Fe^{II}]: UV-vis (10 μM in 9:1 DCM:THF): 419 (Soret; ε = 1.8 × 10^6 M^{-1}cm^{-1}) and 540 (ε = 1.0 × 10^5 M^{-1}cm^{-1}) nm; ^{2}H NMR (9:1 DCM:THF, 193 K): $\delta_{pyrrole}$ = 89.2 ppm.

Low-temperature ^{2}H NMR Spectroscopic Studies. For a typical ^{2}H NMR experiment, 10 mg of **[(THF)$_2$(F_{20}TPP-*d*$_8$)Fe^{II}]** (10 mM) was dissolved in 0.5 mL of 9:1 DCM:THF, and sealed in a 5 mm (outer diameter) NMR tube inside the glovebox. This tube was then stabilized at –90 °C using a liquid nitrogen/acetone cold bath, followed by the addition of $O_{2(g)}$ by means of a 9" needle. Substrate (100 equiv of 3-methylindole in 50 μL of the same solvent) was then added using a Hamilton gas-tight syringe, and was quickly mixed with Ar bubbling. The tube was then transferred into the cryostat of the NMR spectrometer held at –55 °C (Figure 4, black). The major NMR peak observed at –55 °C was centered at 3.2 ppm, indicating the formation of a ferryl intermediate[81] (*Note: the feature at 93.2 ppm is indicative of the presence of a minor paramagnetic component*). The final heme product consists of μ-oxo bridged diferric compound centered at 14.4 ppm, along with a minor monomeric iron(III) hydroxy species with $\delta_{pyrrole}$ = 80.2 ppm (Figure 4, pink).[97-98]

The corresponding authentic ferryl intermediate, **[(THF)(F_{20}TPP-*d*$_8$)Fe^{IV}(O)]**, was prepared by adding 1 equiv of *m*-CPBA to a solution of **[(THF)$_2$(F_{20}TPP-*d*$_8$)Fe^{II}]** in 9:1 DCM:THF, and the NMR data was collected at –55 °C (Figure 4, green; $\delta_{pyrrole}$ = 3.2 ppm); the heme superoxide starting complex, **[(THF)(F_{20}TPP-*d*$_8$)Fe^{III}($O_2^{-\bullet}$)]** (Figure 4, red; $\delta_{pyrrole}$ = 8.8 ppm), was generated by bubbling dry $O_{2(g)}$ into a solution of **[(THF)$_2$(F_{20}TPP-*d*$_8$)Fe^{II}]** (Figure 4, blue; $\delta_{pyrrole}$ = 89.2 ppm) in 9:1 DCM:THF, and the data was collected at –80 °C (Figure 4).

Triphenylphosphine (PPh_3) Oxidation Studies. PPh_3 oxidation to O=PPh_3 was primarily analyzed by ^{31}P NMR spectroscopy. Sample preparation for ^{31}P NMR experiments was carried out as follows: a solution of **[(THF)(TPP)Fe^{III}($O_2^{-\bullet}$)]** was prepared in a 25 mL Schlenk flask using 10 mg of **[(THF)$_2$(TPP)Fe^{II}]** and $O_{2(g)}$ at –80 °C in 9:1 DCM:THF (5 mL). Then, 2.5 mL of 3-methylindole (200 mg, 1.5 mM) and 2.5 mL of PPh_3 (400 mg, 1.5 mM) were added in. This mixture was stirred at –40 °C for 2 hrs. The resultant solution was dried under vacuum, and the residue was redissolved in $CDCl_3$ for NMR analysis (Figure S11). Three control experiments were carried out following similar procedures, but without the addition of (1) **[(THF)$_2$(TPP)Fe^{II}]**, (2) $O_{2(g)}$ and (3) 3-methylindole. The results of these control experiments are summarized in Figures S12 – S14. UV-vis spectroscopic changes for the reaction between **[(B)(TPP)Fe^{III}($O_2^{-\bullet}$)]** (where B = THF or Im) and 3-methylindole was monitored in the presence of 100 equiv of PPh_3, in order to confirm that the formation of the (ferryl) intermediate does occur in the presence of PPh_3. These spectra are summarized in Figure S10.

Bulk Reactions and Characterization of Organic Products. The bulk dioxygenation of all three substrates using **[(THF)(TPP)Fe^{III}($O_2^{-\bullet}$)]** was carried out by a generalized procedure as follows: A 100 mL Schlenk flask containing **[(THF)$_2$(TPP)Fe^{II}]** (100 mg, 0.15 mM) in 9:1 DCM:THF (20 mL) was cooled down in an acetone bath adjusted to –80 °C. Upon temperature equilibration, dioxygen gas (or labeled $^{18}O_{2(g)}$) was bubbled through to form **[(THF)(TPP)Fe^{III}($O_2^{-\bullet}$)]**. Then 3-methylindole (20 mg, 0.15 mM; in 5 mL of 9:1 DCM:THF) was added in, and the reaction mixture was stirred for 2-3 min to mix in the contents. The Schlenk flask was then quickly transferred to another cold bath at –40 °C, and the reaction mixture was stirred for 2 hrs. The final reaction mixture was dried in vacuum, and the final (organic) product was purified by silica gel column chromatography using EtOAc: hexane (1:1) as an eluent. (*Note: When the reaction between **[(THF)(TPP)Fe^{III}($O_2^{-\bullet}$)]** and **2a** was quenched at different time points (15, 30, 45, 60, 90 min), a*

linear increase of product yield was observed before it started plateauing between ~60 – 90 min (Figure S25)).

For LC-MS, an aliquot (20 mL) of each sample was loaded onto a Phenomenex 4.6 x 250mm, 4μm Hydro-RP, 80 Å reverse-phase column (Torrance, CA). A linear gradient of 2-50% acetonitrile in 0.1% formic acid was utilized at a rate of 250 μL/min for 14 mins, then 50-98% acetonitrile-0.1% formic acid was used up to 17.5 min using an Shimadzu Prominence HPLC (Columbia, MD). The column was washed with 98% acetonitrile-0.1% formic acid for 0.5 min, and then re-equilibrated with 2% acetonitrile-0.1% formic acid for 7 min between each sample.

2a: Yield: 6 mg (24%); ^{1}H NMR ($CDCl_3$, 298 K): δ (ppm) = 11.60 (br, 1H; N*H*), 8.76 (d, 1H; Ar-*H*), 8.52 (s, 1H; -C*H*O), 7.93 (d, 1H; Ar-*H*), 7.59 (t, 1H; Ar-*H*), 7.19 (t, 1H; Ar-*H*), 2.69 (s, 3H; -CH_3); ^{13}C NMR (125 MHz, $CDCl_3$, 298 K): δ (ppm) = 202.8, 159.9, 139.8, 135.2, 131.7, 123.1, 122.0, 121.6, 28.57; FT-IR (ATR, cm^{-1}): 1679, 1642, 1603, 1577, 1510, 1451, 1390, 1308, 1251, 1173, 1017, 767; LC-MS: $[M+H]^+$ *m/z* = 164.07 (calc. 164.07).

2b: Yield: 8.5 mg (31%); ^{1}H NMR ($CDCl_3$, 298 K): δ (ppm) = 11.70 (br, 1H; -N*H*), 8.75 (d, 1H; Ar-*H*), 7.90 (d, 1H; Ar-*H*), 7.56 (t, 1H; Ar-*H*), 7.12 (t, 1H; Ar-*H*), 2.67 (s, 3H; -CH_3), 2.24 (s, 3H; -CH_3); ^{13}C NMR (125 MHz, $CDCl_3$, 298 K): δ (ppm) = 202.8, 169.4, 141.0, 135.1, 131.6, 122.3, 121.7, 120.7, 28.6, 25.5; FT-IR (ATR, cm^{-1}): 1686, 1644, 1582, 1516, 1440, 1360, 1300, 1236, 1157, 746; LC-MS: $[M+H]^+$ *m/z* = 178.08 (calc. 178.09).

2c: Yield: 8 mg (18%); ^{1}H NMR ($CDCl_3$, 298 K): δ (ppm) = 11.40 (br, 1H; -N*H*), 8.78 (d, 1H; Ar-*H*), 8.51 (s, 1H; -C*H*O), 7.93 (d, 1H; Ar-*H*), 7.62 (t, 1H; Ar-*H*), 7.21 (t, 1H; Ar-*H*), 6.54 (d, 1H; N-*H*Ac), 4.98 (br, 1H; C-*H*), 3.82-3.72 (m, 2H; -CH_2), 3.79 (s, 3H; -COOCH_3), 2.05 (s, 3H; -NHCOCH_3); ^{13}C NMR (125 MHz, $CDCl_3$, 298 K): δ (ppm) = 202.0, 171.7, 169.9, 159.8, 140.1, 135.9, 131.0, 123.3, 121.7, 120.9, 52.8, 48.2, 41.8, 23.1; FT-IR (ATR, cm^{-1}): 1745, 1697, 1638, 1604, 1580, 1513, 1449, 1430, 1367, 1296, 1201, 984, 751; LC-MS: $[M+H]^+$ *m/z* = 293.11 (calc. 293.11).

Characterization of the Final Heme Product in the Presence and Absence of Imidazole. Authentic **[{(TPP)Fe^{III}}$_2$(*μ*-O)]** and 'naked' **[(THF)$_2$(TPP)Fe^{III}]SbF$_6$** were synthesized as previously reported.[91-92] **[(Im)$_2$(TPP)Fe^{III}]$^+$** was prepared by adding 2.5 equiv of Im to a 0.1 mM 9:1 DCM:THF solution of **[(THF)$_2$(TPP)Fe^{III}]SbF$_6$** at –40 °C (Figures S23 and S24).

ASSOCIATED CONTENT

The Supporting Information is available free of charge on the ACS Publications website at http://pubs.acs.org.

UV-vis, EPR, LC-MS, resonance Raman, ^{1}H NMR, and ^{31}P NMR characterization data related to heme superoxide complexes and their reactivity products (PDF).

AUTHOR INFORMATION

Corresponding Author

*wijeratne@uab.edu

ORCID

Pritam Mondal: 0000-0002-7071-1970
Gayan B. Wijeratne: 0000-0001-7609-6406

Notes

The authors declare no competing financial interest.

ACKNOWLEDGMENT

The University of Alabama at Birmingham (UAB) is gratefully acknowledged for startup funds provided to G. B. W. Authors would like to thank Prof. Ed Solomon, and Anex Jose and Augustin Braun of the Solomon Lab at Stanford University for collecting and interpreting the resonance Raman data included in this study. The authors would also like to thank Prof. Mary Ellen Zvanut (UAB), Dr. Mike Jablonski (UAB), Mayukh Bhadra (Johns Hopkins University), and Landon Wilson (UAB) for assistance with EPR, low-temperature NMR and mass spectrometry/LC-MS experiments. Purchase of the AB Sciex 5600 TripleTOF mass spectrometer in the Targeted Metabolomics and Proteomics Laboratory (TMPL) at UAB came from funds provided by the NCRR grant: S10 RR027822-01. Funds for the operation of TMPL come in part from the UAB O'Brien Acute Kidney Injury Center (P30 DK079337).

REFERENCES

1. Sugimoto, H.; Oda, S.-i.; Otsuki, T.; Hino, T.; Yoshida, T.; Shiro, Y., Crystal structure of human indoleamine 2,3-dioxygenase: Catalytic mechanism of O_2 incorporation by a heme-containing dioxygenase. *Proc. Natl. Acad. Sci. U. S. A.* **2006,** *103*, 2611.
2. Lewis-Ballester, A.; Forouhar, F.; Kim, S.-M.; Lew, S.; Wang, Y.; Karkashon, S.; Seetharaman, J.; Batabyal, D.; Chiang, B.-Y.; Hussain, M.; Correia, M. A.; Yeh, S.-R.; Tong, L., Molecular basis for catalysis and substrate-mediated cellular stabilization of human tryptophan 2,3-dioxygenase. *Sci. Rep.* **2016,** *6*, 35169.
3. Efimov, I.; Basran, J.; Thackray, S. J.; Handa, S.; Mowat, C. G.; Raven, E. L., Chapter 2 - Heme-containing Dioxygenases. In *Adv. Inorg. Chem.*, Eldik, R. v.; Ivanović-Burmazović, I., Eds. Academic Press, London: 2012; Vol. 64, pp 33.
4. Efimov, I.; Basran, J.; Thackray, S. J.; Handa, S.; Mowat, C. G.; Raven, E. L., Structure and Reaction Mechanism in the Heme Dioxygenases. *Biochemistry* **2011,** *50*, 2717.
5. Raven, E. L., A short history of heme dioxygenases: rise, fall and rise again. *J. Biol. Inorg. Chem.* **2016**, 1.
6. Geng, J.; Liu, A., Heme-dependent dioxygenases in tryptophan oxidation. *Arch. Biochem. Biophys.* **2014,** *544*, 18.
7. Ball, H. J.; Jusof, F. F.; Bakmiwewa, S. M.; Hunt, N. H.; Yuasa, H. J., Tryptophan-Catabolizing Enzymes – Party of Three. *Front. Immunol.* **2014,** *5*, 485.
8. Yamamoto, S.; Hayaishi, O., Tryptophan Pyrrolase of Rabbit Intestine: *d*- and *l*-Tryptophan-cleaving Enzyme or Enzymes. *J. Biol. Chem.* **1967,** *242*, 5260.
9. Shimizu, T.; Nomiyama, S.; Hirata, F.; Hayaishi, O., Indoleamine 2,3-dioxygenase. Purification and some properties. *J. Biol. Chem.* **1978,** *253*, 4700.
10. Sono, M.; Roach, M. P.; Coulter, E. D.; Dawson, J. H., Heme-Containing Oxygenases. *Chem. Rev.* **1996,** *96*, 2841.
11. Poulos, T. L., Heme Enzyme Structure and Function. *Chem. Rev.* **2014,** *114*, 3919.
12. Adam, S. M.; Wijeratne, G. B.; Rogler, P. J.; Diaz, D. E.; Quist, D. A.; Liu, J. J.; Karlin, K. D., Synthetic Fe/Cu Complexes: Toward Understanding Heme-Copper Oxidase Structure and Function. *Chem. Rev.* **2018,** *118*, 10840.
13. Thackray, S. J.; Efimov, I.; Raven, E. L.; Mowat, C. G., Chapter 12 Mechanism and Function of Tryptophan and Indoleamine Dioxygenases. In *Iron-Containing Enzymes: Versatile Catalysts of Hydroxylation Reactions in Nature*, The Royal Society of Chemistry, Cambridge: 2011; pp 400.

14. Nelp, M. T.; Zheng, V.; Davis, K. M.; Stiefel, K. J. E.; Groves, J. T., Potent Activation of Indoleamine 2,3-Dioxygenase by Polysulfides. *J. Am. Chem. Soc.* **2019,** *141*, 15288.

15. Lim, C. K.; Bilgin, A.; Lovejoy, D. B.; Tan, V.; Bustamante, S.; Taylor, B. V.; Bessede, A.; Brew, B. J.; Guillemin, G. J., Kynurenine pathway metabolomics predicts and provides mechanistic insight into multiple sclerosis progression. *Sci. Rep.* **2017,** *7*, 41473.

16. Kandanearatchi, A.; Brew, B. J., The kynurenine pathway and quinolinic acid: pivotal roles in HIV associated neurocognitive disorders. *FEBS J.* **2012,** *279*, 1366.

17. Cuartero, M. I.; de la Parra, J.; García-Culebras, A.; Ballesteros, I.; Lizasoain, I.; Moro, M. Á., The Kynurenine Pathway in the Acute and Chronic Phases of Cerebral Ischemia. *Curr. Pharm. Des.* **2016,** *22*, 1060.

18. Linetsky, M.; Raghavan, C. T.; Johar, K.; Fan, X.; Monnier, V. M.; Vasavada, A. R.; Nagaraj, R. H., UVA Light-excited Kynurenines Oxidize Ascorbate and Modify Lens Proteins through the Formation of Advanced Glycation End Products: Implications for Human Lens Aging and Cataract Formation. *J. Biol. Chem.* **2014,** *289*, 17111.

19. Qin, Y.; Wang, N.; Zhang, X.; Han, X.; Zhai, X.; Lu, Y., IDO and TDO as a potential therapeutic target in different types of depression. *Metab. Brain Dis.* **2018,** *33*, 1787.

20. Teraishi, T.; Hori, H.; Sasayama, D.; Matsuo, J.; Ogawa, S.; Ota, M.; Hattori, K.; Kajiwara, M.; Higuchi, T.; Kunugi, H., ^{13}C-tryptophan breath test detects increased catabolic turnover of tryptophan along the kynurenine pathway in patients with major depressive disorder. *Sci. Rep.* **2015,** *5*, 15994.

21. Mazarei, G. a. L., Blair R., Indoleamine 2,3 Dioxygenase as a Potential Therapeutic Target in Huntington's Disease. *J. Huntington's Dis.* **2015,** *4*, 109.

22. Boros, F. A.; Klivényi, P.; Toldi, J.; Vécsei, L., Indoleamine 2,3-dioxygenase as a novel therapeutic target for Huntington's disease. *Expert Opin. Ther. Targets* **2019,** *23*, 39.

23. Szántó, S.; Koreny, T.; Mikecz, K.; Glant, T. T.; Szekanecz, Z.; Varga, J., Inhibition of indoleamine 2,3-dioxygenase-mediated tryptophan catabolism accelerates collagen-induced arthritis in mice. *Arthrit. Res. Ther.* **2007,** *9*, R50.

24. Orabona, C.; Mondanelli, G.; Pallotta, M. T.; Carvalho, A.; Albini, E.; Fallarino, F.; Vacca, C.; Volpi, C.; Belladonna, M. L.; Berioli, M. G.; Ceccarini, G.; Esposito, S. M. R.; Scattoni, R.; Verrotti, A.; Ferretti, A.; De Giorgi, G.; Toni, S.; Cappa, M.; Matteoli, M. C.; Bianchi, R.; Matino, D.; Iacono, A.; Puccetti, M.; Cunha, C.; Bicciato, S.; Antognelli, C.; Talesa, V. N.; Chatenoud, L.; Fuchs, D.; Pilotte, L.; Van den Eynde, B.; Lemos, M. C.; Romani, L.; Puccetti, P.; Grohmann, U., Deficiency of immunoregulatory indoleamine 2,3-dioxygenase 1 in juvenile diabetes. *JCI Insight* **2018,** *3*, e96244.

25. Niño-Castro, A.; Abdullah, Z.; Popov, A.; Thabet, Y.; Beyer, M.; Knolle, P.; Domann, E.; Chakraborty, T.; Schmidt, S. V.; Schultze, J. L., The IDO1-induced kynurenines play a major role in the antimicrobial effect of human myeloid cells against Listeria monocytogenes. *Innate Immun.* **2013,** *20*, 401.

26. Sas, K.; Szabó, E.; Vécsei, L., Mitochondria, Oxidative Stress and the Kynurenine System, with a Focus on Ageing and Neuroprotection. *Molecules* **2018,** *23*, 191.

27. Hornyák, L.; Dobos, N.; Koncz, G.; Karányi, Z.; Páll, D.; Szabó, Z.; Halmos, G.; Székvölgyi, L., The Role of Indoleamine-2,3-Dioxygenase in Cancer Development, Diagnostics, and Therapy. *Front. Immunol.* **2018,** *9*,151.

28. Bilir, C.; Sarisozen, C., Indoleamine 2,3-dioxygenase (IDO): Only an enzyme or a checkpoint controller? *J. Oncol. Sci.* **2017,** *3*, 52.

29. Qian, S.; Zhang, M.; Chen, Q.; He, Y.; Wang, W.; Wang, Z., IDO as a drug target for cancer immunotherapy: recent developments in IDO inhibitors discovery. *RSC Adv.* **2016,** *6*, 7575.

30. Nelp, M. T.; Kates, P. A.; Hunt, J. T.; Newitt, J. A.; Balog, A.; Maley, D.; Zhu, X.; Abell, L.; Allentoff, A.; Borzilleri, R.; Lewis, H. A.; Lin, Z.; Seitz, S. P.; Yan, C.; Groves, J. T., Immune-modulating enzyme indoleamine 2,3-dioxygenase is effectively inhibited by targeting its apo-form. *Proc. Natl. Acad. Sci. U. S. A.* **2018,** *115*, 3249.

31. Coletti, A.; Greco, F. A.; Dolciami, D.; Camaioni, E.; Sardella, R.; Pallotta, M. T.; Volpi, C.; Orabona, C.; Grohmann, U.; Macchiarulo, A., Advances in indoleamine 2,3-dioxygenase 1 medicinal chemistry. *Med. Chem. Comm.* **2017,** *8*, 1378.

32. Labadie, B. W.; Bao, R.; Luke, J. J., Reimagining IDO pathway inhibition in cancer immunotherapy via downstream focus on the tryptophan-kynurenine-aryl hydrocarbon axis. *Clin. Cancer. Res.* **2018**, 1462.

33. Liu, M.; Wang, X.; Wang, L.; Ma, X.; Gong, Z.; Zhang, S.; Li, Y., Targeting the IDO1 pathway in cancer: from bench to bedside. *J. Hematol. Oncol.* **2018,** *11*, 100.

34. Yentz, S.; Smith, D., Indoleamine 2,3-Dioxygenase (IDO) Inhibition as a Strategy to Augment Cancer Immunotherapy. *BioDrugs* **2018,** *32*, 311.

35. Ye, Z.; Yue, L.; Shi, J.; Shao, M.; Wu, T., Role of IDO and TDO in Cancers and Related Diseases and the Therapeutic Implications. *J. Cancer* **2019,** *10*, 2771.

36. Günther, J.; Däbritz, J.; Wirthgen, E., Limitations and Off-Target Effects of Tryptophan-Related IDO Inhibitors in Cancer Treatment. *Front. Immunol.* **2019,** *10*, 1801.

37. Opitz, C. A.; Somarribas Patterson, L. F.; Mohapatra, S. R.; Dewi, D. L.; Sadik, A.; Platten, M.; Trump, S., The therapeutic potential of targeting tryptophan catabolism in cancer. *Br. J. Cancer* **2019,** DOI: 10.1038/s41416-019-0664-6.

38. Hamilton, G. A., Mechanisms of two- and four-electron oxidations catalyzed by some metalloenzymes. *Adv. Enzymol. Relat. Areas Mol. Biol.* **1969,** *32*, 55.

39. Nienhaus, K.; Nienhaus, G. U., Different Mechanisms of Catalytic Complex Formation in Two L-Tryptophan Processing Dioxygenases. *Front. Mol. Biosci.* **2018,** *4*, 94.

40. Chauhan, N.; Thackray, S. J.; Rafice, S. A.; Eaton, G.; Lee, M.; Efimov, I.; Basran, J.; Jenkins, P. R.; Mowat, C. G.; Chapman, S. K.; Raven, E. L., Reassessment of the Reaction Mechanism in the Heme Dioxygenases. *J. Am. Chem. Soc.* **2009,** *131*, 4186.

41. Chung, L. W.; Li, X.; Sugimoto, H.; Shiro, Y.; Morokuma, K., Density Functional Theory Study on a Missing Piece in Understanding of Heme Chemistry: The Reaction Mechanism for Indoleamine 2,3-Dioxygenase and Tryptophan 2,3-Dioxygenase. *J. Am. Chem. Soc.* **2008,** *130*, 12299.

42. Chung, L. W.; Li, X.; Sugimoto, H.; Shiro, Y.; Morokuma, K., ONIOM Study on a Missing Piece in Our Understanding of Heme Chemistry: Bacterial Tryptophan 2,3-Dioxygenase with Dual Oxidants. *J. Am. Chem. Soc.* **2010,** *132*, 11993.

43. Basran, J.; Efimov, I.; Chauhan, N.; Thackray, S. J.; Krupa, J. L.; Eaton, G.; Griffith, G. A.; Mowat, C. G.; Handa, S.; Raven, E. L., The Mechanism of Formation of N-Formylkynurenine by Heme Dioxygenases. *J. Am. Chem. Soc.* **2011,** *133*, 16251.

44. Basran, J.; Booth, E. S.; Lee, M.; Handa, S.; Raven, E. L., Analysis of Reaction Intermediates in Tryptophan 2,3-Dioxygenase: A Comparison with Indoleamine 2,3-Dioxygenase. *Biochemistry* **2016,** *55*, 6743.

45. Lewis-Ballester, A.; Batabyal, D.; Egawa, T.; Lu, C.; Lin, Y.; Marti, M. A.; Capece, L.; Estrin, D. A.; Yeh, S.-R., Evidence for a ferryl intermediate in a heme-based dioxygenase. *Proc. Natl. Acad. Sci. U. S. A.* **2009,** *106*, 17371.

46. Booth, E. S.; Basran, J.; Lee, M.; Handa, S.; Raven, E. L., Substrate Oxidation by Indoleamine 2,3-Dioxygenase: Evidence for a Common Reaction Mechanism. *J. Biol. Chem.* **2015,** *290*, 30924.

47. Yanagisawa, S.; Horitani, M.; Sugimoto, H.; Shiro, Y.; Okada, N.; Ogura, T., Resonance Raman study on the oxygenated and the ferryl-oxo species of indoleamine 2,3-dioxygenase during catalytic turnover. *Faraday Discuss.* **2011,** *148*, 239.

48. Nishinaga, A., Oxygenation Of 3-Substituted Indoles Catalyzed By Co(II)-Schiff's Base Complexes. A Model Catalytic Oxygenation For Tryptophan 2,3-Dioxygenase. *Chem. Lett.* **1975,** *4*, 273.

49. Dufour-Ricroch, M. N.; Gaudemer, A., Reactions de composes indoliques avec l'oxygene moleculaire en presence de metalloporphyrines. *Tetrahedron Lett.* **1976,** *17*, 4079.

50. Uchida, K.; Soma, M.; Naito, S.; Onishi, T.; Tamaru, K., Manganese Phthalocyanine as a Model Of Tryptophan-2,3-Dioxygenase. *Chem. Lett.* **1978,** *7*, 471.

51. Dufour, M. N.; Crumbliss, A. L.; Johnston, G.; Gaudemer, A., Reaction of indoles with molecular oxygen catalyzed by metalloporphyrins. *J. Mol. Catal.* **1980,** *7*, 277.

52. Inada, A.; Nakamura, Y.; Morita, Y., An Effective Dehydrogenation of Indolines to Indoles with Cobalt(II) Schiff's Base Complexes. *Chem. Lett.* **1980,** *9*, 1287.

53. Ohkubo, K.; Sagawa, T.; Ishida, H., Catalytic and stereoselective activities of manganese achiral and chiral porphyrins in dioxygenation of tryptophan derivatives. *Inorg. Chem.* **1992,** *31*, 2682.

54. Yoshida Z I.; Sugimoto, H. O., H., Oxygen activation in oxygenase systems model approach using iron porphyrin. In *Dolphin, D. (Ed) Advances in Chemistry Series*, American Chemical Society: Washington, DC, 1981; Vol. 191 Biomimetic Chemistry; Symposium at The 177th American Chemical Society National Meeting, Honolulu, Hawaii, USA, April 2-5, pp 307.

55. Tajima, K.; Yoshino, M.; Mikami, K.; Edo, T.; Ishizu, K.; Ohya-Nishiguchi, H., Important role of Fe(III)TPP-oxygen-skatole ternary complex in tryptophan dioxygenase model reaction system. *Inorg. Chim. Acta* **1990,** *172*, 83.

56. Oka, S.; Tajima, K.; Sakurai, H., A Chemical Model of Tryptophan 2, 3-Dioxygenase : Reactivity and Formation of a Reactive Intermediate in the Dioxygenation Processes. *Chem. Pharm. Bull. (Tokyo)* **1998,** *46*, 377.

57. Batabyal, D.; Yeh, S.-R., Human Tryptophan Dioxygenase: A Comparison to Indoleamine 2,3-Dioxygenase. *J. Am. Chem. Soc.* **2007,** *129*, 15690.

58. Capece, L.; Lewis-Ballester, A.; Marti, M. A.; Estrin, D. A.; Yeh, S.-R., Molecular Basis for the Substrate Stereoselectivity in Tryptophan Dioxygenase. *Biochemistry* **2011,** *50*, 10910.

59. Capece, L.; Lewis-Ballester, A.; Yeh, S.-R.; Estrin, D. A.; Marti, M. A., Complete Reaction Mechanism of Indoleamine 2,3-Dioxygenase as Revealed by QM/MM Simulations. *J. Phys. Chem. B* **2012,** *116*, 1401.

60. Shin, I.; Ambler, B. R.; Wherritt, D.; Griffith, W. P.; Maldonado, A. C.; Altman, R. A.; Liu, A., Stepwise O-Atom Transfer in Heme-Based Tryptophan Dioxygenase: Role of Substrate Ammonium in Epoxide Ring Opening. *J. Am. Chem. Soc.* **2018,** *140*, 4372.

61. Yanagisawa, S.; Kayama, K. e.; Hara, M.; Sugimoto, H.; Shiro, Y.; Ogura, T., UV Resonance Raman Characterization of a Substrate Bound to Human Indoleamine 2,3-Dioxygenase 1. *Biophys. J.* **2019**, *117*, 706.

62. Huang, X.; Groves, J. T., Oxygen Activation and Radical Transformations in Heme Proteins and Metalloporphyrins. *Chem. Rev.* **2018,** *118*, 2491.

63. Fukuzumi, S.; Lee, Y. M.; Nam, W., Structure and reactivity of the first-row d-block metal-superoxo complexes. *Dalton Trans.* **2019,** *48*, 9469.

64. Jasniewski, A. J.; Que, L., Dioxygen Activation by Nonheme Diiron Enzymes: Diverse Dioxygen Adducts, High-Valent Intermediates, and Related Model Complexes. *Chem. Rev.* **2018,** *118*, 2554.

65. Lai, W.; Shaik, S., Can Ferric-Superoxide Act as a Potential Oxidant in P450cam? QM/MM Investigation of Hydroxylation, Epoxidation, and Sulfoxidation. *J. Am. Chem. Soc.* **2011,** *133*, 5444.

66. Chung, L. W.; Li, X.; Hirao, H.; Morokuma, K., Comparative Reactivity of Ferric-Superoxo and Ferryl-Oxo Species in Heme and Non-Heme Complexes. *J. Am. Chem. Soc.* **2011,** *133*, 20076.

67. Singha, A.; Dey, A., Hydrogen atom abstraction by synthetic heme ferric superoxide and hydroperoxide species. *Chem. Commun.* **2019,** *55*, 5591.

68. Sharma, S. K.; Rogler, P. J.; Karlin, K. D., Reactions of a heme-superoxo complex toward a cuprous chelate and $^{\bullet}NO_{(g)}$: C*c*O and NOD chemistry. *J. Porphyr. Phthalocyanines* **2015,** *19*, 352.

69. Collman, J. P.; Gagne, R. R.; Reed, C.; Halbert, T. R.; Lang, G.; Robinson, W. T., Picket fence porphyrins. Synthetic models for oxygen binding hemoproteins. *J. Am. Chem. Soc.* **1975,** *97*, 1427.

70. Sharma, S. K.; Kim, H.; Rogler, P. J.; A. Siegler, M.; Karlin, K. D., Isocyanide or nitrosyl complexation to hemes with varying tethered axial base ligand donors: synthesis and characterization. *J. Biol. Inorg. Chem.* **2016,** *21*, 729.

71. Kurtikyan, T. S.; Ford, P. C., Hexacoordinate oxy-globin models Fe(Por)(NH_3)(O_2) react with NO to form only the nitrato analogs Fe(Por)(NH_3)(η^1-ONO_2), even at ~100 K. *Chem. Commun.* **2010,** *46*, 8570.

72. Burke, J. M.; Kincaid, J. R.; Peters, S.; Gagne, R. R.; Collman, J. P.; Spiro, T. G., Structure-sensitive resonance Raman bands of tetraphenyl and "picket fence" porphyrin-iron complexes, including an oxyhemoglobin analog. *J. Am. Chem. Soc.* **1978,** *100*, 6083.

73. Garcia-Bosch, I.; Adam, S. M.; Schaefer, A. W.; Sharma, S. K.; Peterson, R. L.; Solomon, E. I.; Karlin, K. D., A "Naked" Fe^{III}-(O_2^{2-})-Cu^{II} Species Allows for Structural and Spectroscopic Tuning of Low-Spin Heme-Peroxo-Cu Complexes. *J. Am. Chem. Soc.* **2015,** *137*, 1032.

74. Sharma, S. K.; Schaefer, A. W.; Lim, H.; Matsumura, H.; Moënne-Loccoz, P.; Hedman, B.; Hodgson, K. O.; Solomon, E. I.; Karlin, K. D., A Six-Coordinate Peroxynitrite Low-Spin Iron(III) Porphyrinate Complex—The Product of the Reaction of Nitrogen Monoxide ($\cdot NO_{(g)}$) with a Ferric-Superoxide Species. *J. Am. Chem. Soc.* **2017,** *139*, 17421.

75. The exact assignments of the additional isotope sensitive features centered at 970 and 1130 cm^{-1} require much rigorous spectroscopic and computational studies (i.e., normal coordinate analysis) than presented in the current study.

76. Cady, S. G.; Sono, M., 1-methyl-dl-tryptophan, *β*-(3-benzofuranyl)-dl-alanine (the oxygen analog of tryptophan), and *β*-[3-benzo(b)thienyl]-dl-alanine (the sulfur analog of tryptophan) are competitive inhibitors for indoleamine 2,3-dioxygenase. *Arch. Biochem. Biophys.* **1991,** *291*, 326.

77. Ehudin, M. A.; Gee, L. B.; Sabuncu, S.; Braun, A.; Moënne-Loccoz, P.; Hedman, B.; Hodgson, K. O.; Solomon, E. I.; Karlin, K. D., Tuning the Geometric and Electronic Structure of Synthetic High-Valent Heme Iron(IV)-Oxo Models in the Presence of a Lewis Acid and Various Axial Ligands. *J. Am. Chem. Soc.* **2019,** *141*, 5942.

78. Pan, Z.; Newcomb, M., Kinetics and Mechanism of Oxidation Reactions of Porphyrin−Iron(IV)−Oxo Intermediates. *Inorg. Chem.* **2007,** *46*, 6767.

79. Balch, A. L.; La Mar, G. N.; Latos-Grazynski, L.; Renner, M. W.; Thanabal, V., Nuclear magnetic resonance studies of axial amine coordination in synthetic ferryl, $(Fe^{IV}O)^{2+}$, porphyrin complexes and in ferryl myoglobin. *J. Am. Chem. Soc.* **1985,** *107*, 3003.

80. Ehudin, M. A.; Quist, D. A.; Karlin, K. D., Enhanced Rates of C–H Bond Cleavage by a Hydrogen-Bonded Synthetic Heme High-Valent Iron(IV) Oxo Complex. *J. Am. Chem. Soc.* **2019,** *141*, 12558.

81. Ghiladi, R. A.; Kretzer, R. M.; Guzei, I.; Rheingold, A. L.; Neuhold, Y.-M.; Hatwell, K. R.; Zuberbühler, A. D.; Karlin, K. D., (F_8TPP)Fe^{II}/O_2 Reactivity Studies {F_8TPP = Tetrakis(2,6-difluorophenyl)porphyrinate(2−)}: Spectroscopic (UV−Visible and NMR) and Kinetic Study of Solvent-Dependent (Fe/O_2 = 1:1 or 2:1) Reversible O_2-Reduction and Ferryl Formation. *Inorg. Chem.* **2001,** *40*, 5754.

82. Shirin, Z.; S. Borovik, A.; G. Young Jr, V., Synthesis and structure of a Mn^{III}(OH) complex generated from dioxygen. *Chem. Commun.* **1997**, 1967.

83. Yan, J. J.; Kroll, T.; Baker, M. L.; Wilson, S. A.; Decréau, R.; Lundberg, M.; Sokaras, D.; Glatzel, P.; Hedman, B.; Hodgson, K. O.; Solomon, E. I., Resonant inelastic X-ray scattering determination of the electronic structure of oxyhemoglobin and its model complex. *Proc. Natl. Acad. Sci. U. S. A.* **2019,** *116*, 2854.

84. Makino, R.; Obayashi, E.; Hori, H.; Iizuka, T.; Mashima, K.; Shiro, Y.; Ishimura, Y., Initial O_2 Insertion Step of the Tryptophan Dioxygenase Reaction Proposed by a Heme-Modification Study. *Biochemistry* **2015,** *54*, 3604.

85. Neither the authentic ferryl species nor the diferric oxo-bridged compound was observed to be competent of indole dioxygenation (Figure S22). Furthermore, "free" superoxide (generated by KO_2 and 18-crown-6) in solution (in the absence of heme) failed to oxidize indoles under the same reaction conditions as the bulk reactions reported herein.

86. Chin, D.-H.; La Mar, G. N.; Balch, A. L., Mechanism of autoxidation of iron(II) porphyrins. Detection of a peroxo-bridged iron(III) porphyrin dimer and the mechanism of its thermal decomposition to the oxo-bridged iron(III) porphyrin dimer. *J. Am. Chem. Soc.* **1980,** *102*, 4344.

87. Chin, D.-H.; Del Gaudio, J.; La Mar, G. N.; Balch, A. L., Detection and characterization of the long-postulated iron-dioxygen-iron intermediate in the autoxidation of ferrous porphyrins. *J. Am. Chem. Soc.* **1977,** *99*, 5486.

88. Peters, M. K.; Röhricht, F.; Näther, C.; Herges, R., One-Pot Approach to Chlorins, Isobacteriochlorins, Bacteriochlorins, and Pyrrocorphins. *Org. Lett.* **2018,** *20*, 7879.

89. Muresan, A. Z.; Thamyongkit, P.; Diers, J. R.; Holten, D.; Lindsey, J. S.; Bocian, D. F., Regiospecifically α-^{13}C-Labeled Porphyrins for Studies of Ground-State Hole Transfer in Multiporphyrin Arrays. *J. Org. Chem.* **2008,** *73*, 6947.

90. Song, X.; Xu, C.; Du, D.; Zhao, Z.; Zhu, D.; Wang, M., Ring-Opening Diarylation of Siloxydifluorocyclopropanes by Ag(I) Catalysis: Stereoselective Construction of 2-Fluoroallylic Scaffold. *Org. Lett.* **2017,** *19*, 6542.

91. Helms, J. H.; Ter Haar, L. W.; Hatfield, W. E.; Harris, D. L.; Jayaraj, K.; Toney, G. E.; Gold, A.; Mewborn, T. D.; Pemberton, J. E., Effect of meso substituents on exchange-coupling interactions in μ-oxo iron(III) porphyrin dimers. *Inorg. Chem.* **1986,** *25*, 2334.

92. Quinn, R.; Nappa, M.; Valentine, J. S., New five- and six-coordinate imidazole and imidazolate complexes of ferric tetraphenylporphyrin. *J. Am. Chem. Soc.* **1982,** *104*, 2588.

93. Wang, J.; Schopfer, M. P.; Puiu, S. C.; Sarjeant, A. A. N.; Karlin, K. D., Reductive Coupling of Nitrogen Monoxide (•NO) Facilitated by Heme/Copper Complexes. *Inorg. Chem.* **2010,** *49*, 1404.

94. Nam, W.; Lim, M. H.; Moon, S. K.; Kim, C., Participation of Two Distinct Hydroxylating Intermediates in Iron(III) Porphyrin Complex-Catalyzed Hydroxylation of Alkanes. *J. Am. Chem. Soc.* **2000,** *122*, 10805.

95. Schappacher, M.; Weiss, R.; Montiel-Montoya, R.; Trautwein, A.; Tabard, A., Formation of an iron(IV)-oxo "picket-fence" porphyrin derivative via reduction of the ferrous dioxygen adduct and reaction with carbon dioxide. *J. Am. Chem. Soc.* **1985,** *107*, 3736.

96. Nam, W.; Lim, M. H.; Oh, S.-Y., Effect of Anionic Axial Ligands on the Formation of Oxoiron(IV) Porphyrin Intermediates. *Inorg. Chem.* **2000,** *39*, 5572.

97. Jayaraj, K.; Gold, A.; Toney, G. E.; Helms, J. H.; Hatfield, W. E., Preparation and characterization of the μ-oxo dimer and hydroxo complexes of (tetrakis(pentafluorophenyl)porphinato)iron(III). *Inorg. Chem.* **1986,** *25*, 3516.

98. Cheng, R. J.; Latos-Grazynski, L.; Balch, A. L., Preparation and characterization of some hydroxy complexes of iron(III) porphyrins. *Inorg. Chem.* **1982,** *21*, 2412.

TOC Figure: